

Adsorption of ^4He on a single C_{60}

Leszek Szybisz^{1,2,*} and Ignacio Urrutia^{1,+}

¹*Laboratorio TANDAR, Departamento de Física, Comisión Nacional de Energía Atómica,
Av. del Libertador 8250, RA-1429 Buenos Aires, Argentina*

²*Departamento de Física, Facultad de Ciencias Exactas y Naturales,
Universidad de Buenos Aires, Ciudad Universitaria, RA-1428 Buenos Aires, Argentina*

(March 22, 2022)

Abstract

The adsorption of ^4He inside and outside a single fullerene C_{60} is studied. A physisorption potential is proposed. The energetics and structural features of $\text{C}_{60}\text{-}^4\text{He}_N$ clusters are investigated. Particular attention is paid to the growth of the highly pronounced layered density profile. The evolution towards bulk liquid and surface thickness at the free interface are discussed.

FILENAME: fuller.tex

PACS numbers: 61.20.-p, 68.03.Cd

I. INTRODUCTION

Since the discovery of the fullerenes and nanotubes a large amount of work has been devoted to study properties of such systems.¹ In particular, in the case of nanotubes the adsorption of quantum fluids has been thoroughly investigated.² The physisorption potential for such systems has been modeled several years ago by Stan and Cole.³ Calculations performed for ^4He adsorbed into carbon nanotubes have shown interesting features.^{4,5} It was found that inside tubes of radius $\lesssim 7\text{\AA}$, besides the formation of a shell phase located at about 3\AA from the wall, a quasi-one-dimensional structure along the cylinder axis is also developed. These sorts of quasi-one-dimensional structures are of theoretical interest.^{6,7} On the other hand, the shell phase located close to the wall exhibits a surface density in agreement with the experimental value^{8,9} obtained for monolayer completion density on graphite (see Table I). Moreover, adsorption in bundles of nanotubes have been also studied showing a rich pattern of phase transitions.^{10,11}

On the other hand, hitherto there is no study of the adsorption of ^4He onto C_{60} in the literature. One expects that the cloud of ^4He surrounding this fullerene will exhibit a shell structure of the type found for helium clusters doped with atomic or molecular impurities.^{12–18} It is of interest to determine how pronounced will be the layering as well as to estimate the shells' surface densities in order to make a comparison with results for other geometries mentioned above. By looking at the behavior of these $\text{C}_{60}\text{-}^4\text{He}_N$ clusters for increasing number of helium atoms, N , one may search whether growth instabilities like those found in the case of planar graphite substrates¹⁹ are also present in this case. Furthermore, one may search for what is going on when the clusters approach bulk liquid. Other issue to be examined is the liquid-vacuum interface thickness. There is a current interest in this observable²⁰ and experimental data for spherical and planar helium systems are available.^{21,22} Moreover, since the field is open for exploration new unexpected features may appear.

The paper is organized in the following way. In Sec. II we outline the model and construct

the physisorption potential for the interaction between C_{60} and ^4He atoms. Numerical results are presented in Sec. III together with the discussion of the whole picture exhibited by the systems. Section IV is devoted to final remarks.

II. THE MODEL

A. Theoretical Framework

The adsorption properties at $T = 0$ K may be studied by analyzing the grand thermodynamic potential

$$\Omega = E_{\text{gs}} - \mu N, \quad (2.1)$$

where E_{gs} is the ground-state energy, μ the chemical potential, and N the number of particles of the adsorbed fluid. In the present work we adopted a density functional (DF) approach, which has proven to be a successful tool for treating this kind of quantum many-body problems. In such a theory the ground-state energy of an interacting N -body system of ^4He atoms, confined by an adsorbate-substrate potential $U_{\text{sub}}(\mathbf{r})$, may be written as

$$E_{\text{gs}} = -\frac{\hbar^2}{2m} \int d\mathbf{r} \sqrt{\rho(\mathbf{r})} \nabla^2 \sqrt{\rho(\mathbf{r})} + \int d\mathbf{r} \rho(\mathbf{r}) e_{sc}(\mathbf{r}) + \int d\mathbf{r} \rho(\mathbf{r}) U_{\text{sub}}(\mathbf{r}), \quad (2.2)$$

where $\rho(\mathbf{r})$ is the one-body density and $e_{sc}(\mathbf{r})$ the self-correlation energy per particle. The density profile $\rho(\mathbf{r})$ is determined from the Euler-Lagrange (EL) equation derived from the condition

$$\frac{\delta \Omega}{\delta \rho(\mathbf{r})} = \frac{\delta \{ E_{\text{gs}}[\rho, \nabla \rho] - \mu N \}}{\delta \rho(\mathbf{r})} = 0. \quad (2.3)$$

In the present work, we adopted for ^4He the non-local density functional (NLDF) proposed by the Orsay-Trento (OT) collaboration,²³ with only one change which consist in neglecting the non-local gradient correction to the kinetic energy term as it was done by

Mayol *et al.*²⁴ Although this kind of functionals is known, we present a summary for the sake of completeness. The self-correlation energy is expressed as

$$e_{sc}(\mathbf{r}) = \frac{1}{2} \int d\mathbf{r}' \rho(\mathbf{r}') V_l^{\text{OT}}(|\mathbf{r} - \mathbf{r}'|) + \frac{c'_4}{2} [\bar{\rho}(\mathbf{r})]^2 + \frac{c''_4}{3} [\bar{\rho}(\mathbf{r})]^3, \quad (2.4)$$

with $c'_4 = -2.411857 \times 10^4 \text{ K}\text{\AA}^6$ and $c''_4 = 1.858496 \times 10^6 \text{ K}\text{\AA}^9$. The two-body interaction, $V_l^{\text{OT}}(|\mathbf{r} - \mathbf{r}'|)$, was taken as the ^4He - ^4He Lennard-Jones (LJ) potential screened in a simple way at distances shorter than a characteristic distance h_{OT}

$$V_l^{\text{OT}}(r) = \begin{cases} 4\epsilon_{\text{LJ}} \left[\left(\frac{\sigma_{\text{LJ}}}{r} \right)^{12} - \left(\frac{\sigma_{\text{LJ}}}{r} \right)^6 \right] & \text{if } r \geq h_{\text{OT}}, \\ 0 & \text{if } r < h_{\text{OT}}, \end{cases} \quad (2.5)$$

with the standard de Boer and Michels parameters,²⁵ namely, well depth $\epsilon_{\text{LJ}} = 10.22 \text{ K}$ and hard core radius $\sigma_{\text{LJ}} = 2.556 \text{ \AA}$, in addition, the screening distance $h_{\text{OT}} = 2.190\,323 \text{ \AA}$.

Quantity $\bar{\rho}(\mathbf{r})$ is the “coarse-grained density” defined as the straight average of $\rho(\mathbf{r})$ over a sphere centered at \mathbf{r} and with a radius equal to the screening distance h_{OT}

$$\bar{\rho}(\mathbf{r}) = \int d\mathbf{r}' \rho(\mathbf{r}') \mathcal{W}(|\mathbf{r} - \mathbf{r}'|), \quad (2.6)$$

where $\mathcal{W}(|\mathbf{r} - \mathbf{r}'|)$ is the normalized step function

$$\mathcal{W}(|\mathbf{r} - \mathbf{r}'|) = \begin{cases} \frac{3}{4\pi h_{\text{OT}}^3} & \text{if } |\mathbf{r} - \mathbf{r}'| \leq h_{\text{OT}}, \\ 0 & \text{if } |\mathbf{r} - \mathbf{r}'| > h_{\text{OT}}. \end{cases} \quad (2.7)$$

B. The physisorption potential

The fullerene C_{60} is to a very good approximation a spherical system.¹ For constructing the potential due to this carbon structure we followed the procedure already applied in the case of a single nanotube.³ So, we suppose that an adsorbed ^4He atom located at \vec{r} , measured

from the C_{60} center, interacts with a single substrate C atom of the spherical shell at \vec{r}' via an isotropic LJ pair potential with standard parameters $\varepsilon_{\text{CHe}} = 16.24$ K and $\sigma_{\text{CHe}} = 2.74$ Å taken from Ref. 9. Next, we consider a spherically averaged potential by assuming that the C atoms are uniformly distributed over the spherical surface of radius R_{full} . Under these conditions, the total effect of all carbon atoms is given by

$$U_{\text{sub}}(r) = 8 \pi \varepsilon_{\text{CHe}} \Theta_s R_{\text{full}}^2 \times \int_0^\pi \left[\left(\frac{\sigma_{\text{CHe}}}{|\vec{r} - \vec{r}'|} \right)^{12} - \left(\frac{\sigma_{\text{CHe}}}{|\vec{r} - \vec{r}'|} \right)^6 \right] \sin \theta d\theta. \quad (2.8)$$

Here, $\Theta_s = N_c/(4\pi R_{\text{full}}^2)$ is the uniform surface density of C atoms. After some straightforward algebra the expression for $U_{\text{sub}}(r)$ inside the fullerene can be cast into the form

$$U_{\text{sub}}(r) = 2 N_c \varepsilon_{\text{CHe}} \times \left[\left(\frac{\sigma_{\text{CHe}}}{R_{\text{full}}} \right)^{12} M_6(\nu) - \left(\frac{\sigma_{\text{CHe}}}{R_{\text{full}}} \right)^6 M_3(\nu) \right], \quad (2.9)$$

where $M_n(\nu)$ stands for the integral

$$\begin{aligned} M_n(\nu) &= \int_0^\pi \frac{\sin \varphi d\varphi}{(1 + \nu^2 - 2\nu \cos \varphi)^n} \\ &= \int_{-1}^1 \frac{dx}{(1 + \nu^2 + 2\nu x)^n} \\ &= \frac{1}{2(n-1)\nu} \left[\frac{1}{(1-\nu)^{2(n-1)}} - \frac{1}{(1+\nu)^{2(n-1)}} \right], \end{aligned} \quad (2.10)$$

with $\nu = r/R_{\text{full}}$. On the other hand, the adsorption potential outside of the fullerene becomes

$$U_{\text{sub}}(r) = 2 N_c \varepsilon_{\text{CHe}} \times \left[\left(\frac{\sigma_{\text{CHe}}}{r} \right)^{12} M_6(\nu) - \left(\frac{\sigma_{\text{CHe}}}{r} \right)^6 M_3(\nu) \right], \quad (2.11)$$

with $\nu = R_{\text{full}}/r$. Since in the limit $\nu \rightarrow 0$ holds

$$M_n(\nu \rightarrow 0) = 2, \quad (2.12)$$

one gets the correct result at the C_{60} center

$$U_{\text{sub}}(r=0) = N_c 4 \varepsilon_{LJ} \left[\left(\frac{\sigma_{\text{CHe}}}{R_{\text{full}}} \right)^{12} - \left(\frac{\sigma_{\text{CHe}}}{R_{\text{full}}} \right)^6 \right], \quad (2.13)$$

and also the appropriate asymptotic behavior very far away from the fullerene

$$U_{\text{sub}}(r \gg R_{\text{full}}) = N_c 4 \varepsilon_{LJ} \left[\left(\frac{\sigma_{\text{CHe}}}{r} \right)^{12} - \left(\frac{\sigma_{\text{CHe}}}{r} \right)^6 \right]. \quad (2.14)$$

We expect that the resulting potential would give a reliable description of the main features of the systems.

III. RESULTS AND ANALYSIS

In the case of a spherical symmetry the variation of Eq. (2.3) leads to the following Hartree like equation for the square root of the one-body helium density

$$\begin{aligned} -\frac{\hbar^2}{2m} \left(\frac{d^2}{dr^2} + \frac{2}{r} \frac{d}{dr} \right) \sqrt{\rho(r)} \\ + \left[V_H(r) + U_{\text{sub}}(r) \right] \sqrt{\rho(r)} = \mu \sqrt{\rho(r)}, \end{aligned} \quad (3.1)$$

which also determines μ . Here $V_H(\mathbf{r})$ is a Hartree mean-field potential given by the first functional derivative of the total correlation energy $E_{sc}[\rho]$

$$V_H(\mathbf{r}) = \frac{\delta E_{sc}[\rho]}{\delta \rho(\mathbf{r})} = \frac{\delta}{\delta \rho(\mathbf{r})} \int d\mathbf{r}' \rho(\mathbf{r}') e_{sc}(\mathbf{r}'). \quad (3.2)$$

The expression derived for the spherically symmetric $V_H(r)$ is given in the Appendix. Equation (3.1) was solved at a fixed number of helium atoms

$$N = 4 \pi \int_0^\infty r^2 dr \rho(r). \quad (3.3)$$

The calculations has been carried out for $R_{\text{full}} = 3.53 \text{ \AA}$ (cf. Ref. 1) that for $N_c = 60$ leads to $\Theta_s = 0.38 \text{ \AA}^{-2}$ in agreement with the surface density used for nanotubes. As shown in Fig. 1 the difference between the inner and outer potential depths is dramatic.

A. Inner Atom

Since the radius is very small there is enough room for only one ^4He atom inside the fullerene. The solution for such a system is obtained from Eq. (3.1) by using $U_{\text{sub}}(r)$ given by Eq. (2.9) and setting to zero the correlation energy. So, the problem is reduced to a Schrödinger equation.

Figure 2 shows the energies and wave functions for the lowest two eigenstates together with the inner potential. A remarkable feature of these results is that inside of the fullerene a helium atom is extremely strongly bound with a ground-state energy $E_{\text{gs}} = E_0 = -592$ K.

B. The $\text{C}_{60}\text{-}^4\text{He}_N$ clusters

Adsorption on the external side of the fullerene has been studied by solving the complete Eq. (3.1) for systems up to $N = 1600$ ^4He atoms. In this approach we neglect the zero-point motion of the fullerene and treat it as a body with infinite mass. It has been established that this is a reasonable description in the case of helium clusters doped with sulfur hexafluoride molecules (SF_6).^{16–18} One expects that this approach be even better for C_{60} because it is a heavier and stronger attractor.

The energy per particle, $e = E_{\text{gs}}/N$, and the chemical potential, μ , are plotted in Fig. 3 as a function of N . The size of these results can be understood by taking into account that the adsorption potential outside presents a well depth of about 100 K, being much smaller than inside as shown in Fig. 1. Examples of density profiles are displayed in Fig. 4. Small $\text{C}_{60}\text{-}^4\text{He}_N$ clusters exhibit a typical layered structure. Two well defined layers are developed at $N \simeq 160$. For larger systems begins the transition towards bulk liquid.

Let us first focus the attention on small systems. After a small region where $\Omega > 0$ (for $N \lesssim 20$) begins the growth of a stable monolayer film. For $N \gtrsim 60$ starts the formation of the second layer and μ exhibits a kink. At this point one must be careful because a growth instability similar to that found for films adsorbed on strongly attractive planar substrates¹⁹

might appear. This kind of instability would cause a jump of N in the adsorption isotherm. We have checked the possible presence of such a feature by increasing N in steps of $\Delta N = 1$. It was found that μ is always an increasing function of N as shown in Fig. 5. In addition, we analyzed whether the unstable regime is close. A transition to instabilities may be induced by increasing the strength of the C_{60} - ^4He interaction. In turn, this may be achieved by either changing the potential parameters or going to fullerenes with more carbon atoms, i.e., larger radii. Since we would like to stick C_{60} , the former way for enhancing the attraction of the potential was selected. Calculations have been carried out for $\sigma_{\text{CHe}} = 2.98 \text{ \AA}$, this value has been widely used in the past for the graphite-helium interaction (see discussion in Ref. 26) and it increases about 10% the well depth. The new plateau corresponding to the growth of the second layer is shown in Fig. 5. From this drawing one concludes that in this case μ is also an increasing function of N indicating stability of the solutions. So, we can state that the solutions for $\sigma_{\text{CHe}} = 2.74 \text{ \AA}$ do not undergo growth instability and, in addition, that the unstable regime is not close to the adopted scenario.

We shall now examine the surface density of the first two layers. Experimentally it has been determined that for a planar substrate of graphite the adsorbed superfluid ^4He presents two well defined layers with coverages $n_{s1} = 0.115 \text{ \AA}^{-2}$ and $n_{s2} = 0.093 \text{ \AA}^{-2}$ for the first and second layer, respectively.^{8,9} In the present work, surface densities were evaluated according to

$$n_{si} = \frac{N_i}{4\pi \langle R_i \rangle^2}, \quad (3.4)$$

where $\langle R_i \rangle$ is the location of the i -layer and N_i its number of particles. Looking at Fig. 4 one realizes that the first layer is well defined, it is centered at $\langle R_1 \rangle = 6.41 \text{ \AA}$ and a simple integration yields $N_1 = 57$ leading to $n_{s1} = 0.110 \text{ \AA}^{-2}$. Although the position of the second layer may be easily obtained, $\langle R_2 \rangle = 9.35 \text{ \AA}$, the evaluation of N_2 is not straightforward because the right-hand side region of the peak is not clearly exhibited. By taking into account the superposition of tails of the second and third peaks we estimated $N_2 = 90$ which gives $n_{s2} = 0.082 \text{ \AA}^{-2}$. In order to facilitate the comparison all the results

for the surface density mentioned along the paper are collected in Table I. A glance at this table indicates a fair agreement between calculated and experimental data, although the present value of n_{s2} is slightly smaller than the experimental one, presumably due to the curvature of C_{60} .

For large N the systems evolve towards bulk liquid. This is merely an expected behavior. The real theoretical prediction is how rapidly the clusters approach that limit when N is increased. In addition, the comparison with other doped clusters becomes of interest. In Fig. 6 we plotted e and μ as a function of $N^{-1/3}$, which is the appropriate expansion parameter for spherical drops. To fix ideas we recall that e and μ for free spherical ^4He clusters obey the following asymptotic laws:

$$e_{\text{As}} = \frac{E_{\text{gs}}}{N} = e_B + \left(\frac{36\pi}{\rho_0^2} \right)^{1/3} \sigma_\infty N^{-1/3}, \quad (3.5)$$

and

$$\mu_{\text{As}} = \left(\frac{dE_{\text{gs}}}{dN} \right)_{\text{As}} = e_B + 2 \left(\frac{4\pi}{3\rho_0^2} \right)^{1/3} \sigma_\infty N^{-1/3}. \quad (3.6)$$

Here $e_B = \mu_0 = -7.15$ K, $\rho_0 = 0.021836 \text{ \AA}^{-3}$, and $\sigma_\infty = 0.274 \text{ K \AA}^{-2}$ (see Refs. 27–31). These straight lines are included in Fig. 6. The results displayed in this figure indicate that μ reaches much more rapidly the asymptotic trend than e . At about $N \simeq 500$ the chemical potential lies, in practice, on the straight line given by Eq. (3.6). At this value of N the slope of μ changes indicating a phase transition to a metastable regime. The behavior of e is biased by the very strongly attractive potential. The dashed curve indicates how e might attain e_B . This curve was obtained by fitting data for $N \geq 500$ to

$$e = e_B + \left(\frac{36\pi}{\rho_0^2} \right)^{1/3} \sigma_\infty N^{-1/3} + a_c N^{-2/3} + a_0 N^{-1}, \quad (3.7)$$

which yielded $a_c = 0.2$ K and $a_0 = -3316.4$ K. The large negative value of a_0 is caused by the strong attraction exerted by C_{60} . Furthermore, it is important to notice that these coefficients also explain the behavior of μ . In this region of N the chemical potential obeys Eq. (3.6) due to the facts that a_c is small and the huge a_0 does not contribute because $\mu = dE_{\text{gs}}/dN$.

The trend of e towards the asymptotic law given by Eq. (3.5) is noticeable delayed in comparison with diffusion Monte Carlo (DMC) results¹² for $\text{SF}_6\text{-}^4\text{He}_N$ clusters. It should be mentioned that these DMC values were reproduced fairly well by NLDF evaluations (see Fig. 1 in Ref. 18) as well as by hypernetted chain calculations (cf. Fig. 12 in Ref. 15). Perhaps it is worthwhile to notice that the latter figure also indicates that helium doped with atomic impurities like Ne, Ar, Kr, and Xe reaches even more rapidly the asymptotic behavior for e than the $\text{SF}_6\text{-}^4\text{He}_N$ clusters do. On the other hand, from a glance at Fig. 3 of Ref. 18 one could conjecture that the collective energy of the dipole mode for $\text{C}_{60}\text{-}^4\text{He}_N$ clusters with N even a few hundreds bigger than 1000 would still not approach zero. This means that the instability scenario for the dopant would not be reached for $N = 1600$ yet.

Let us briefly refer to the entrance to the bulk regime. From the fit to Eq. (3.7) it is possible to determine that the crossing between e and μ takes place at $N^{-1/3} \simeq 0.041$, see also Fig. 6. This indicates that at $N \simeq 14500$ the bulk could be reached. It would be interesting to find out whether the collective energy of the dipole mode for such large systems is still positive.

Finally, we shall focus our attention on the width of the liquid-vacuum interface. At this interface, the density profile of ^4He changes continuously from liquid density ρ_ℓ to zero over a distance of some ångströms. The width W of a surface is defined as the distance in which the density decreases from $0.9\rho_\ell$ to $0.1\rho_\ell$. For consistency with other studies we adopted $\rho_\ell = \rho_0$. The analysis was centered on systems with $N \geq 600$ because for such clusters the oscillations of $\rho(r)$ close to the free interface are already damped enough. The present results for W are compared in Fig. 7 with values calculated for free ^4He droplets²⁰ and experimental data.^{21,22} The results obtained in the measurement of large droplets published in Ref. 21 are represented by the reported mean thickness $W = 6.4 \pm 1.3$ Å. In the case of Ref. 22 only the two data included by the authors in the abstract are shown. Since the latter values correspond to rather broad planar films, we plotted them schematically close to origin for the abscissa. The overall agreement exhibited in Fig. 7 is good.

IV. FINAL REMARKS

The main results of this investigation about C_{60} - ${}^4\text{He}_N$ clusters may be summarized in the following way. Only one ${}^4\text{He}$ atom may be put inside of this fullerene and its binding energy is very large. The energetics of the adsorption on the external side was studied and the structure of the films was determined.

The evolution of the systems for increasing N does not exhibit any growth instability after the completion of the first layer and, in addition, the unstable scenario is not close. The surface density of the first two layers are in fair agreement with experimental data for planar graphite. The analysis of the transition towards bulk liquid as a function of N shows that μ attains more rapidly the asymptotic behavior than e . Results obtained from a fit of e account for this feature. The C_{60} - ${}^4\text{He}_N$ clusters approach the bulk regime much slower than helium clusters doped with a SF_6 molecule.

The surface thickness at the liquid-vacuum interface obtained for rather large clusters matches reasonably well with theoretical evaluations for free helium spheres and experimental data for droplets and films.

For the future work it remains the study of excitations, which may give information on the location of C_{60} . Furthermore, this issue is also a challenge for experimental work as well as Monte Carlo simulations due to the fact that such investigations may also shed some light on the importance of the zero-point motion of this heavy dopant. Moreover, it would be exciting to look for a possible levitation of C_{60} in bulk helium.

ACKNOWLEDGMENTS

The authors acknowledge enlightening discussions with E.S. Hernández and thank H. Bonadeo and E. Burgos for providing valuable information. This work was supported in part by the Ministry of Culture and Education of Argentina through Grants PICT-2000-03-08450 from ANPCYT and No. X103 from University of Buenos Aires.

APPENDIX: HARTREE MEAN-FIELD POTENTIAL

In this Appendix we compile the relevant expressions derived in the adopted NLDF approach. For a spherical geometry the definition of the Hartree mean-field of Eq. (3.2) leads to

$$\begin{aligned}
 V_H(r) = & \int d\mathbf{r}' \rho(r') V_l^{\text{OT}}(|\mathbf{r} - \mathbf{r}'|) \\
 & + \frac{c'_4}{2} [\bar{\rho}(r)]^2 + \frac{c''_4}{3} [\bar{\rho}(r)]^3 \\
 & + \int d\mathbf{r}' \rho(r') \{ c'_4 \bar{\rho}(r') + c''_4 [\bar{\rho}(r')]^2 \} \mathcal{W}(|\mathbf{r} - \mathbf{r}'|) .
 \end{aligned} \tag{A1}$$

Let us first provide the expressions of the contributions involving the “coarse-grained density” $\bar{\rho}(r)$, *i.e.*,

$$\bar{\rho}(r) = \int d\mathbf{r}' \rho(r') \mathcal{W}(|\mathbf{r} - \mathbf{r}'|) , \tag{A2}$$

and

$$\bar{\rho}_V(r) = \int d\mathbf{r}' \rho(r') [\bar{\rho}(r')]^n \mathcal{W}(|\mathbf{r} - \mathbf{r}'|) . \tag{A3}$$

Both these integrals may be cast into the form

$$\bar{\mathcal{R}}(r) = \frac{3}{4\pi h_{\text{OT}}^3} \int d\mathbf{r}' \mathcal{R}(r') \Theta(h_{\text{OT}} - |\mathbf{r} - \mathbf{r}'|) . \tag{A4}$$

After introducing spherical coordinates and taking into account that the step function is symmetric in the azimuthal angle φ , the integration over this variable yields

$$\begin{aligned}
 \bar{\mathcal{R}}(r) = & \frac{3}{2 h_{\text{OT}}^3} \int_{r'_{\min}}^{r'_{\max}} r'^2 dr' \mathcal{R}(r') \int_0^{\theta_{\max}} \sin \theta d\theta \\
 & \times \Theta[h_{\text{OT}}^2 - r^2 - r'^2 + 2 r r' \cos \theta] .
 \end{aligned} \tag{A5}$$

Since we shall treat helium systems located at $r > h_{\text{OT}}$, the limits for the radial integral become $r'_{\min} = r - h_{\text{OT}}$ and $r'_{\max} = r + h_{\text{OT}}$. Furthermore, the step function sets

$$\cos \theta_{\max} = \frac{r^2 + r'^2 - h_{\text{OT}}^2}{2 r r'} . \tag{A6}$$

Hence, one gets²⁰

$$\bar{\mathcal{R}}(r) = \frac{3}{4r h_{\text{OT}}} \int_{r-h_{\text{OT}}}^{r+h_{\text{OT}}} r' dr' \mathcal{R}(r') \left[1 - \left(\frac{r-r'}{h_{\text{OT}}} \right)^2 \right]. \quad (\text{A7})$$

On the other hand, the integration of the screened LJ potential contributing to Eq. (A1) for $r \geq h_{\text{OT}}$ leads to

$$\begin{aligned} V_H^{\text{LJScr}}(r) &= \int d\mathbf{r}' \rho(r') V_l^{\text{OT}}(|\mathbf{r} - \mathbf{r}'|) \\ &= \frac{4\pi\epsilon_{\text{LJ}} \sigma_{\text{LJ}}^2}{r} \left\{ \int_0^{r-h_{\text{OT}}} + \int_{r+h_{\text{OT}}}^{\infty} \right\} r' dr' \rho(r') \\ &\quad \times \left\{ \frac{1}{5} \left[\left(\frac{\sigma_{\text{LJ}}}{r-r'} \right)^{10} - \left(\frac{\sigma_{\text{LJ}}}{r+r'} \right)^{10} \right] \right. \\ &\quad \left. - \frac{1}{2} \left[\left(\frac{\sigma_{\text{LJ}}}{r-r'} \right)^4 - \left(\frac{\sigma_{\text{LJ}}}{r+r'} \right)^4 \right] \right\} \\ &\quad + \frac{4\pi\epsilon_{\text{LJ}} \sigma_{\text{LJ}}^2}{r} \int_{r-h_{\text{OT}}}^{r+h_{\text{OT}}} r' dr' \rho(r') \left\{ \frac{1}{5} \left[\left(\frac{\sigma_{\text{LJ}}}{h_{\text{OT}}} \right)^{10} \right. \right. \\ &\quad \left. \left. - \left(\frac{\sigma_{\text{LJ}}}{r+r'} \right)^{10} \right] - \frac{1}{2} \left[\left(\frac{\sigma_{\text{LJ}}}{h_{\text{OT}}} \right)^4 - \left(\frac{\sigma_{\text{LJ}}}{r+r'} \right)^4 \right] \right\}. \end{aligned} \quad (\text{A8})$$

It is worthwhile to notice that we expressed these quantities in a rather simple compact form similar to Eq. (2.16) written in Ref. 32 for planar films instead of adopting the expansion in terms of Legendre polynomials proposed in Ref. 13. The latter procedure is more appropriate for studying excitations of a given system.

REFERENCES

- * Also at the Carrera del Investigador Científico of the Consejo Nacional de Investigaciones Científicas y Técnicas, Av. Rivadavia 1917, RA-1033 Buenos Aires, Argentina.
- ⁺ Also at the Comisión de Investigaciones Científicas de la Prov. de Buenos Aires, Calle 526 entre 10 y 11, RA-1900 La Plata, Argentina.
- ¹ M. S. Dresselhaus, G. Dresselhaus, and P. E. Eklund, *Science of Fullerenes and Carbon Nanotubes* (Academic, New York, 1997).
- ² M. M. Calbi, M. W. Cole, S. M. Gatica, M. J. Bojan, and G. Stan, Rev. Mod. Phys. **73**, 857 (2001).
- ³ G. Stan and M. W. Cole, Surf. Sci. **395**, 280 (1998).
- ⁴ S. M. Gatica, G. Stan, M. M. Calbi, J. K. Johnson, and M. W. Cole, J. Low Temp. Phys. **120**, 337 (2000).
- ⁵ S. M. Gatica, E. S. Hernández, and L. Szybisz, submitted to Phys. Rev. B.
- ⁶ E. Krotscheck and M. D. Miller, Phys. Rev. B **60**, 13038 (1999).
- ⁷ M. Boninsegni and S. Moroni, J. Low Temp. Phys. **118**, 1 (2000).
- ⁸ H. J. Lauter, H. Godfrin, V. P. Franck, P. Lederer, in *Excitations in Two-Dimensional and Three-Dimensional Quantum Fluids*, NATO ASI Series, Ser. B, Vol. 257 (Plenum, New York, 1991), pp. 419ff.
- ⁹ L. W. Bruch, M. W. Cole, and E. Zaremba, *Physical Adsorption* (Oxford Univ. Press, Oxford, 1997).
- ¹⁰ M. W. Cole, V. H. Crespi, G. Stan, C. Ebner, J. M. Hartman, S. Moroni, and M. Boninsegni, Phys. Rev. Lett. **84**, 3883 (2000).
- ¹¹ S. M. Gatica, M. M. Calbi, and M. W. Cole, Phys. Rev. E **65**, 061605 (2002).

- ¹² R. N. Barnett and K. B. Whaley, J. Chem. Phys. **99**, 9730 (1993).
- ¹³ M. Barranco and E. S. Hernández, Phys. Rev. B **49**, 12078 (1994).
- ¹⁴ E. S. Hernández and M. Barranco, Phys. Rev. B **51**, 9364 (1995).
- ¹⁵ S. A. Chin and E. Krotscheck, Phys. Rev. B **52**, 10405 (1995).
- ¹⁶ M. Hartmann, R. B. Miller, J. P. Toennies, and A. Vilesov, Phys. Rev. Lett. **75**, 1566 (1995).
- ¹⁷ M. A. McMahon, R. N. Barnett, and K. B. Whaley, J. Chem. Phys. **104**, 5080 (1996).
- ¹⁸ S. M. Gatica, E. S. Hernández, and M. Barranco, J. Chem. Phys. **107**, 927 (1997).
- ¹⁹ B. E. Clements, E. Krotscheck, and H. J. Lauler, Phys. Rev. Lett. **70**, 1287 (1993).
- ²⁰ L. Szybisz and I. Urrutia, eprint cond-mat/0305662, to be published in Phys. Rev. B (2003).
- ²¹ J. Harms, J. P. Toennies, and F. Dalfovo, Phys. Rev. B **58**, 3341 (1998).
- ²² K. Penanen, M. Fukuto, R. K. Heilmann, I. F. Silvera, and P. S. Pershan, Phys. Rev. B **62**, 9621 (2000).
- ²³ F. Dalfovo, A. Lastri, L. Pricauenko, S. Stringari, and J. Treiner, Phys. Rev. B **52**, 1193 (1995).
- ²⁴ R. Mayol, M. Pi, M. Barranco, and F. Dalfovo, Phys. Rev. Lett. **87**, 145301 (2001).
- ²⁵ J. de Boer and A. Michels, Physica **6**, 945 (1938).
- ²⁶ M. W. Cole, D. R. Frankl, and D. L. Goodstein, Rev. Mod. Phys. **53**, 199 (1981).
- ²⁷ S. Stringari and J. Treiner, Phys. Rev. B **36**, 8369 (1987).
- ²⁸ H. M. Guo, D. O. Edwards, R. E. Sarwinski, and J. T. Tough, Phys. Rev. Lett. **27**, 1259 (1971).

- ²⁹ D. O. Edwards and W. F. Saam, in *Progress in Low Temperature Physics*, edited by D. F. Brewer (North-Holland, Amsterdam, 1978) Vol. 7A, Chap. 4.
- ³⁰ M. Iino, M. Suzuki, and A. J. Ikushima, J. Low Temp. Phys. **61**, 155 (1985).
- ³¹ P. Roche, G. Deville, N. J. Appleyard, and F. I. B. Williams, J. Low Temp. Phys. **106**, 565 (1997).
- ³² J. Dupont-Roc, M. Himbert, N. Pavloff, and J. Treiner, J. Low Temp. Phys. **81**, 31 (1990).

TABLES

TABLE I. Surface density of ^4He layers adsorbed on planar graphite compared with results for helium shells confined into a cylindrical carbon nanotube and adsorbed onto a spherical C_{60} .

Geometry	Method	$n_{s1} [\text{\AA}^{-2}]$	$n_{s2} [\text{\AA}^{-2}]$	Ref.
Planar	Experiment	0.115	0.093	8, 9
Cylindrical	Theory	0.113		4
Spherical	Theory	0.110	0.082	PW ^a

^a PW stands for present work.

FIGURES

FIG. 1. The left-most curve is the potential for a ^4He atom inside the fullerene evaluated with Eq. (2.9). The right-most curve is the potential for a ^4He atom outside of the fullerene evaluated with Eq. (2.11). Notice that the surface of C_{60} is located at $r = 3.53 \text{ \AA}$.

FIG. 2. Energies and wave functions of the two lowest eigenstates for a single ^4He atom inside C_{60} . Quantities $\psi_n(r)$ are in arbitrary scale. The bold curve is the potential.

FIG. 3. Energy per particle and chemical potential for $\text{C}_{60}\text{-}^4\text{He}_N$ clusters as a function of the number of helium atoms.

FIG. 4. Density profiles for a series of $\text{C}_{60}\text{-}^4\text{He}_N$ clusters. Results for $N = 50, 100, 150, 200, 300, 400, \dots$, up to 1600 are displayed.

FIG. 5. Chemical potential as a function of N . The plateau corresponding to the growth of the second layer is shown for two values of σ_{CHe} (see text).

FIG. 6. Energy per particle (filled circles) and chemical potential (empty circles) as a function of $N^{-1/3}$. Asymptotic laws for e and μ are displayed. The dashed curve indicates the trend of e towards the asymptotic $e_B = \mu_0$. Stars are DMC values for the energy per particle of $\text{SF}_6\text{-}^4\text{He}_N$ clusters taken from Ref. 12, the dot-dashed curve stands only to guide the eye.

FIG. 7. Thickness of the free surface as a function of $N^{-1/3}$. Triangles are data for $\text{C}_{60}\text{-}^4\text{He}_N$ clusters with $N \geq 600$. Full circles are results for free ^4He droplets from Ref. 20 and the solid curve indicates the trend of these data. The “otimes” (\otimes) and the “oplus” (\oplus) are experimental values from Refs. 21 and 22, respectively.

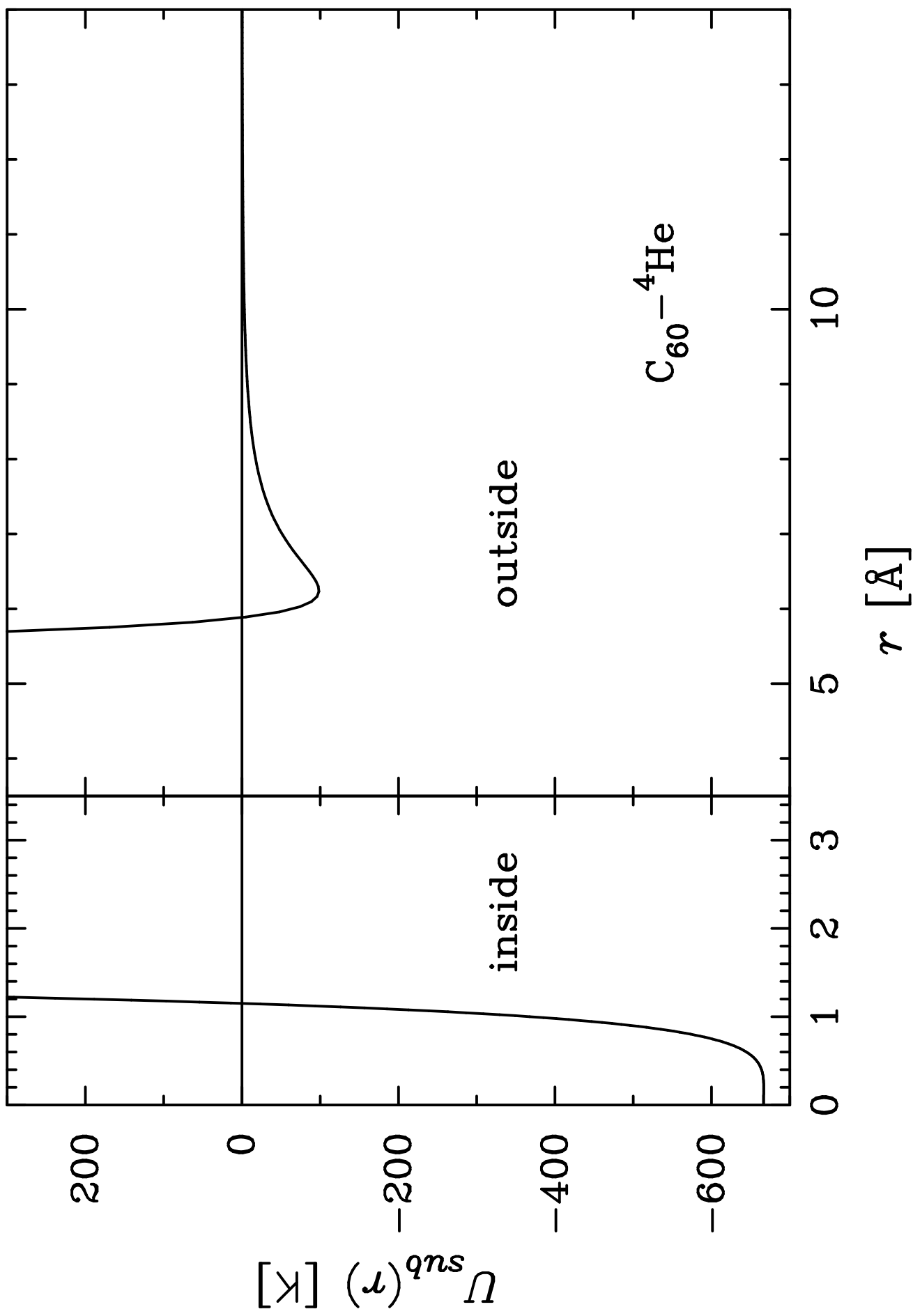


Fig. 1 $C_{60}-^4He_N$

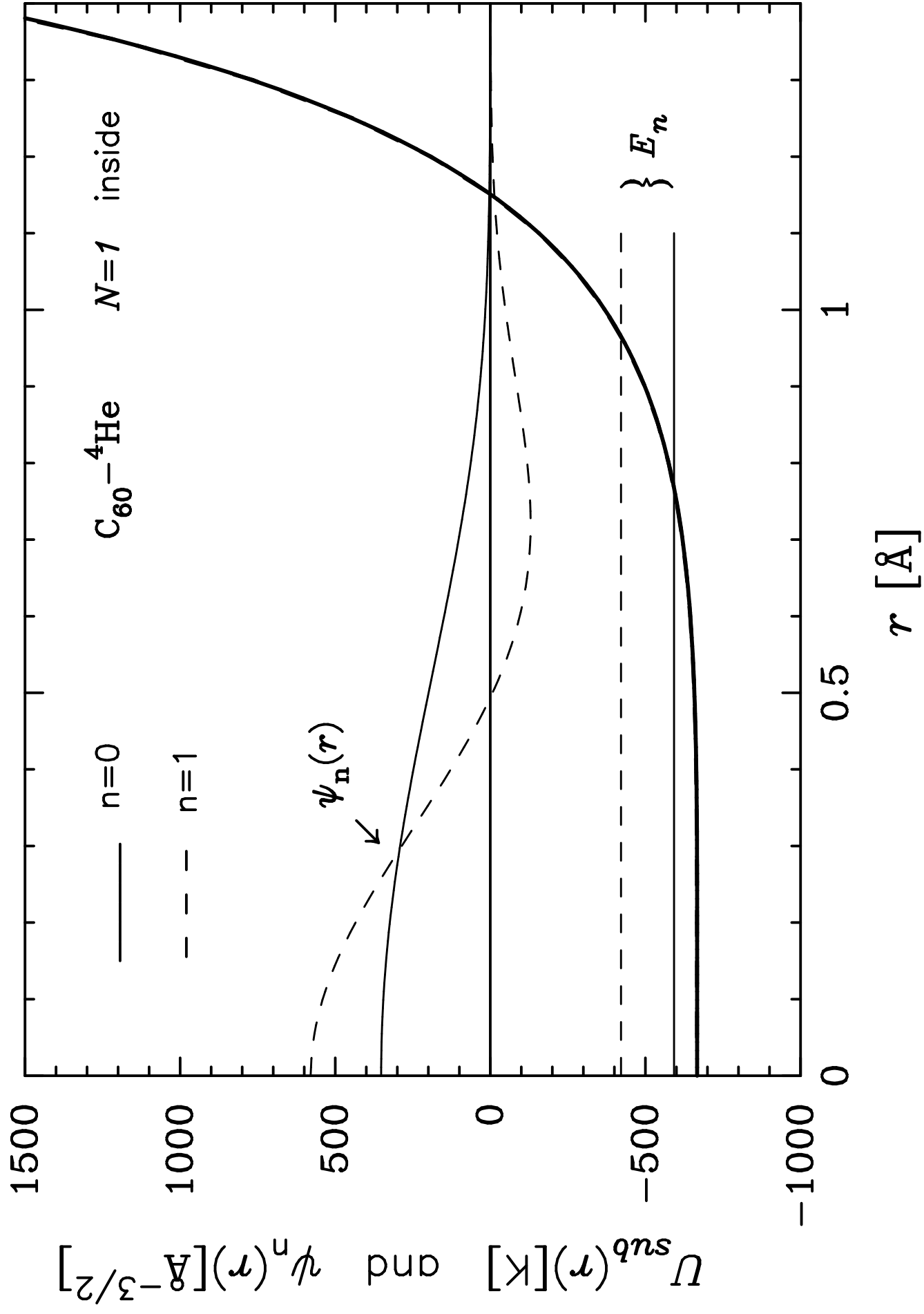


Fig. 2 $^4\text{He}/C_{60}$

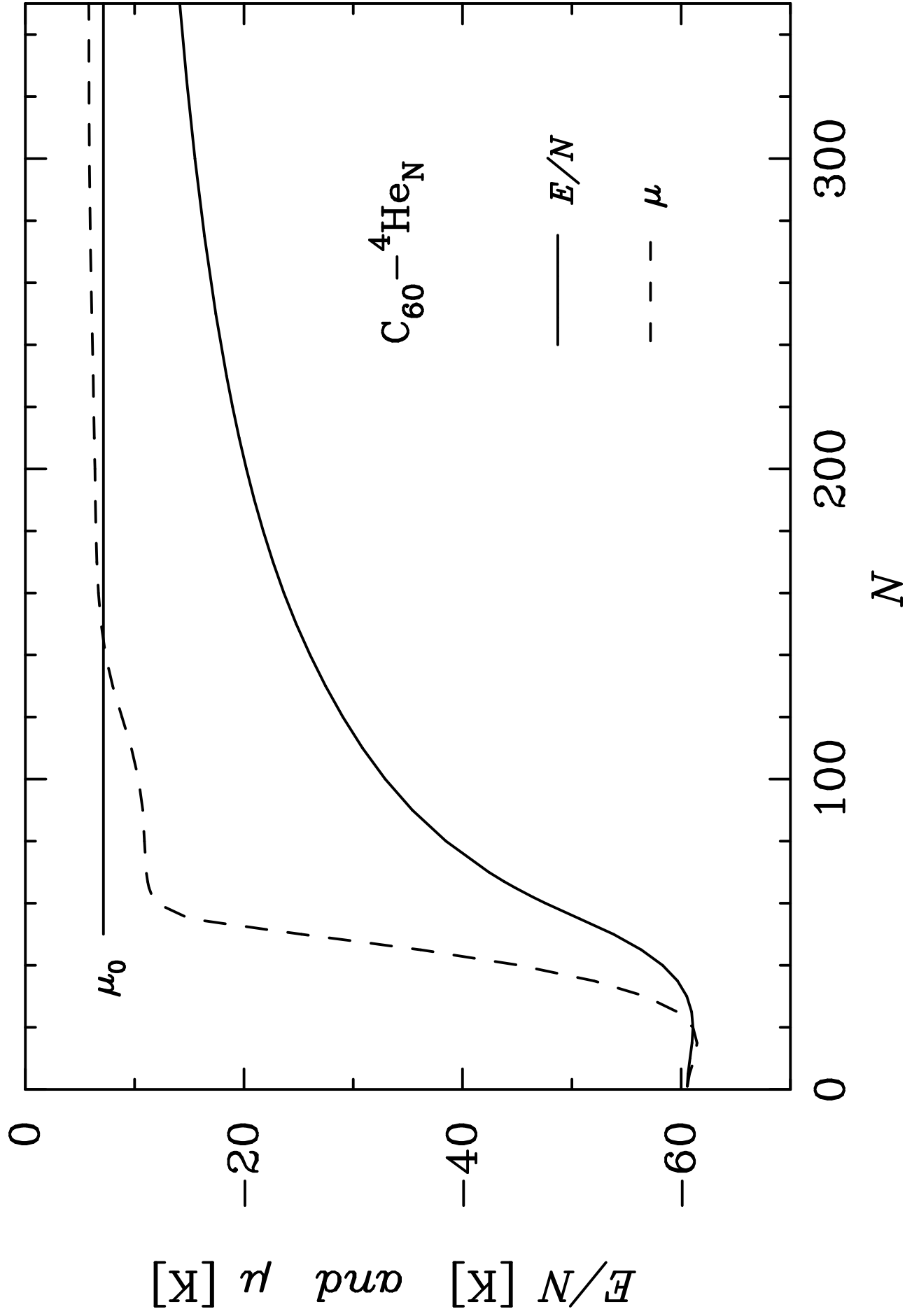


Fig. 3 ${}^4\text{He}/C_{60}$

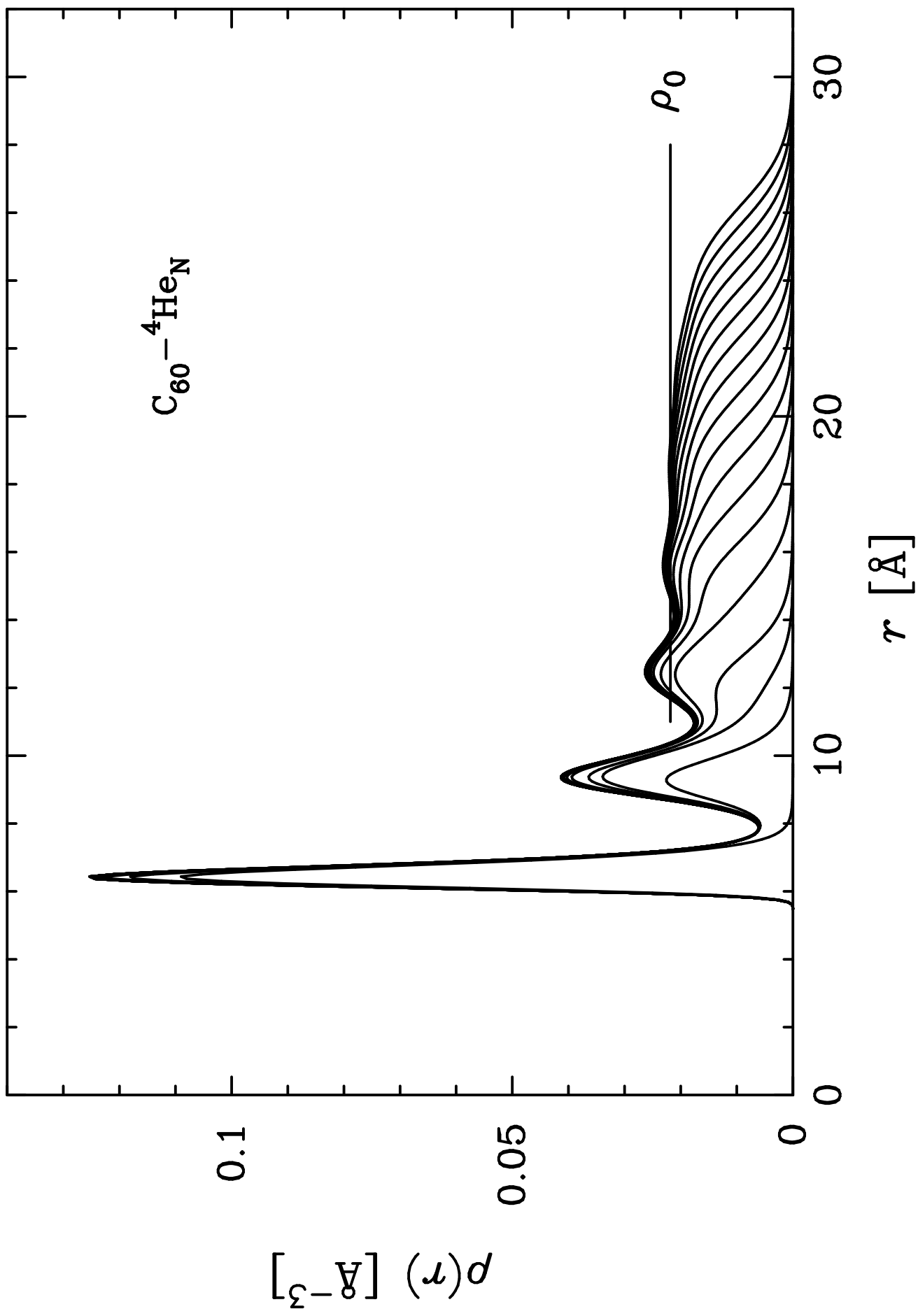


Fig. 4 ${}^4\text{He}/\text{C}_{60}$

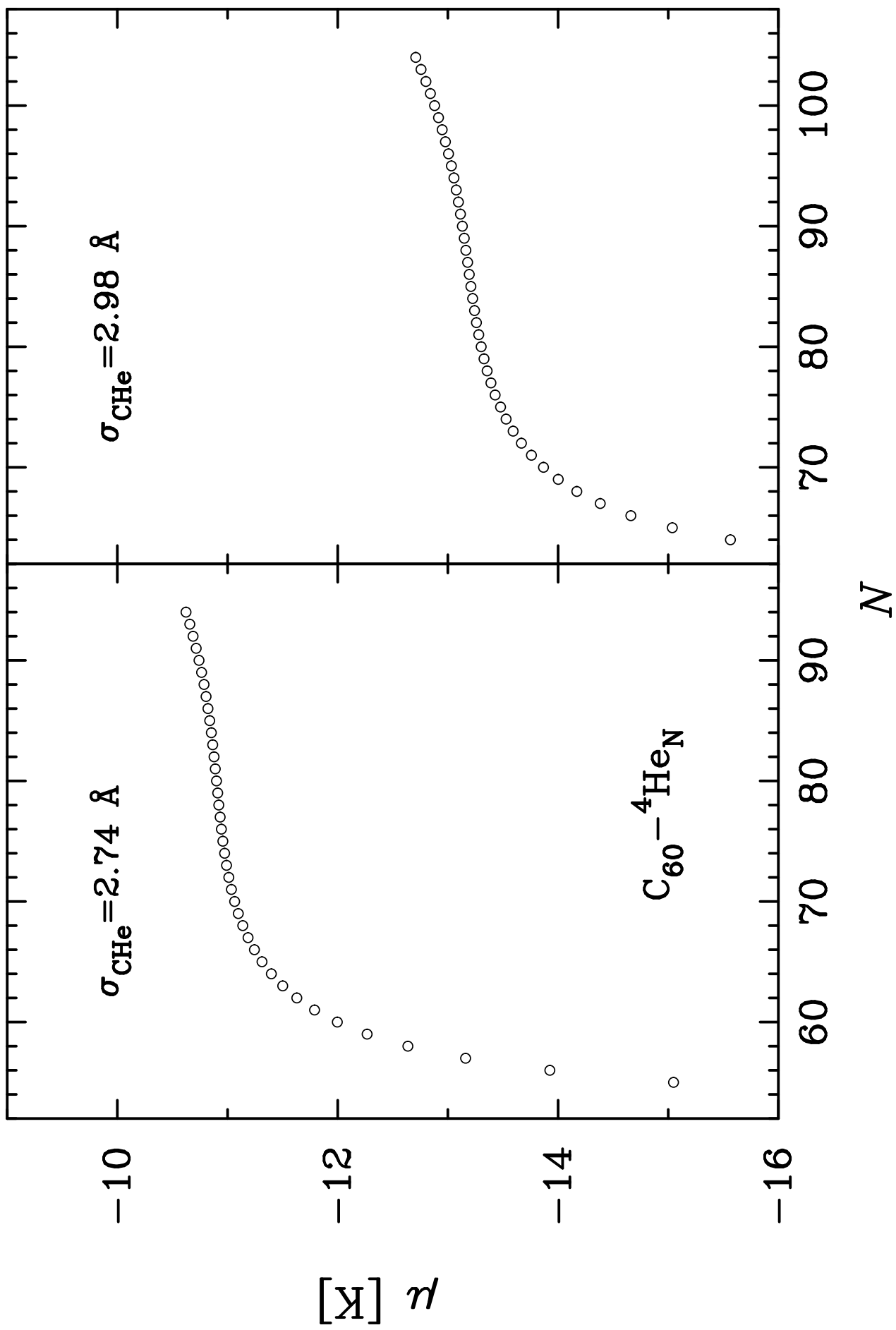


Fig. 5 $^4\text{He}/C_{60}$

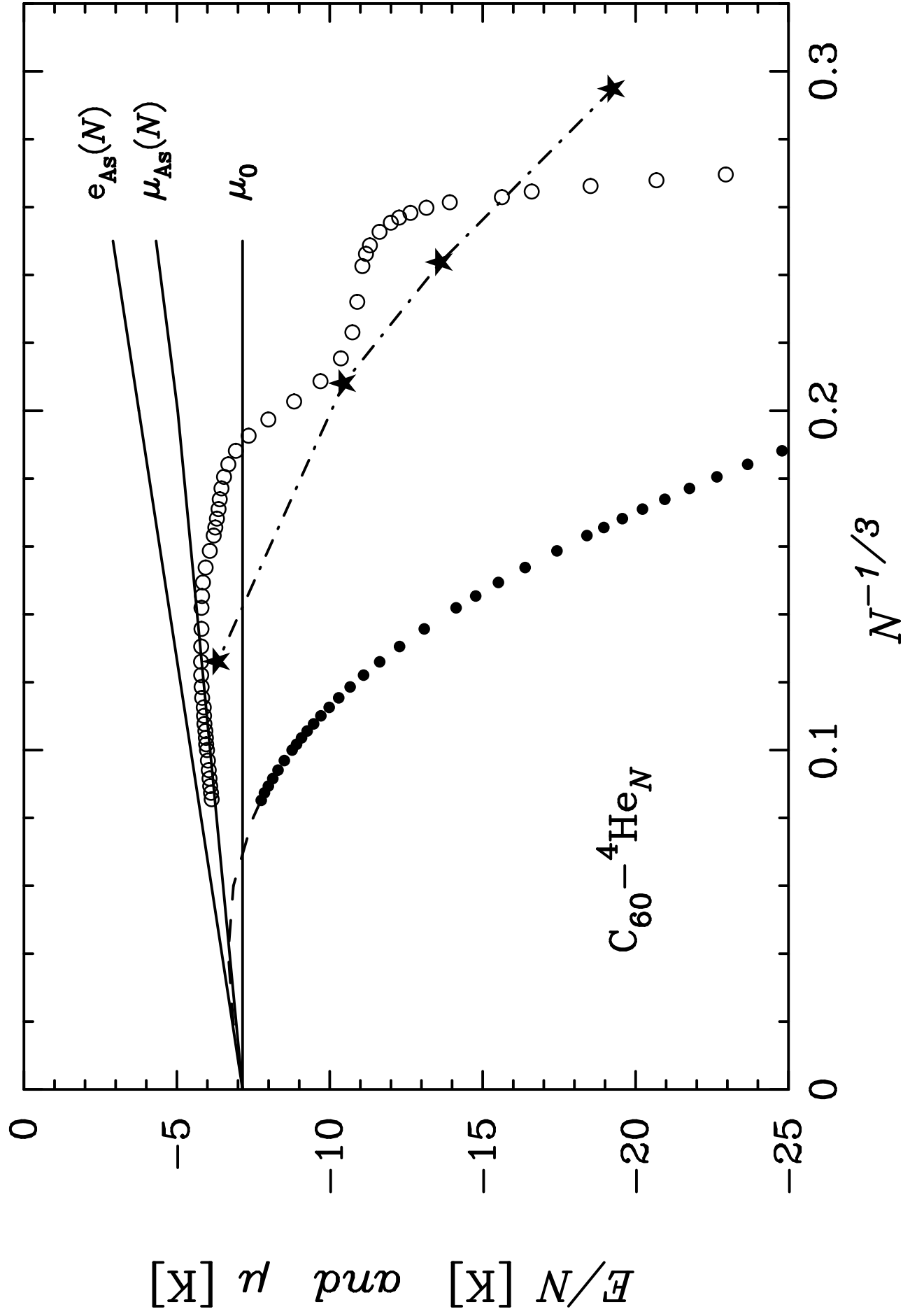


Fig. 6 $^4He/C_{60}$

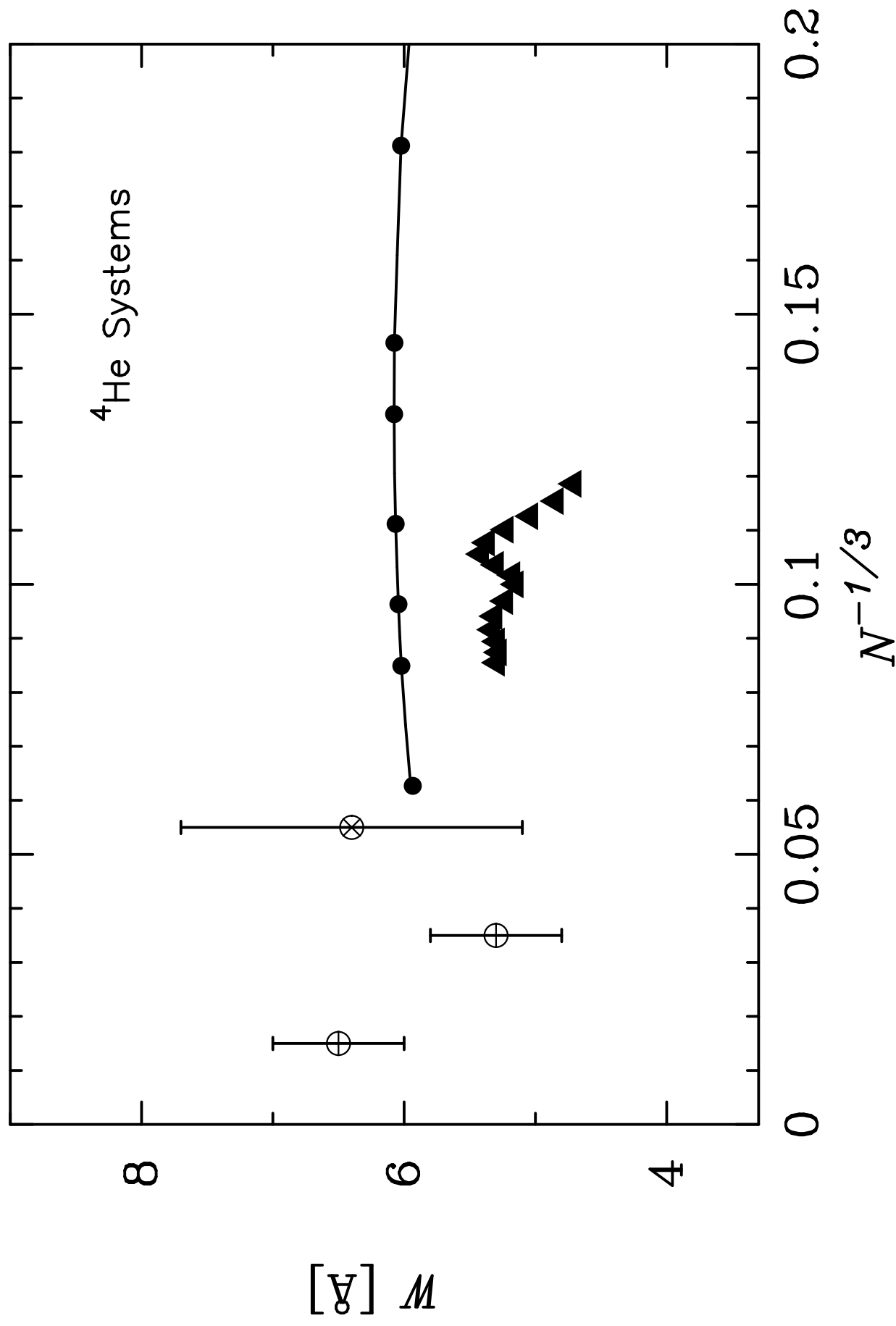


Fig. 7 Width $C_{60}-^4\text{He}_N$